The Astrophysical Journal Supplement Series, 226:14 (8pp), 2016 October doi:10.3847/0067-0049/226/2/14

EXTENDED RELATIVISTIC CONFIGURATION INTERACTION AND MANY-BODY PERTURBATION CALCULATIONS OF SPECTROSCOPIC DATA FOR THE $N \leqslant 6$ CONFIGURATIONS IN Ne-LIKE IONS BETWEEN Cr XV AND Kr XXVII

K. Wang[1,2,3], Z. B. Chen[4], R. Si[3], P. Jönsson[5], J. Ekman[5], X. L. Guo[3,6], S. Li[2], F. Y. Long[2], W. Dang[1], X. H. Zhao[1], R. Hutton[3], C. Y. Chen[3], J. Yan[2,7,8], and X. Yang[9]

[1] Hebei Key Lab of Optic-electronic Information and Materials, The College of Physics Science and Technology, Hebei University, Baoding 071002, China
[2] Institute of Applied Physics and Computational Mathematics, Beijing 100088, China; yan_jun@iapcm.ac.cn
[3] Shanghai EBIT Lab, Institute of Modern Physics, Department of Nuclear Science and Technology, Fudan University, Shanghai 200433, China; chychen@fudan.edu.cn
[4] College of Science, National University of Defense Technology, Changsha 410073, China
[5] Group for Materials Science and Applied Mathematics, Malmö University, SE-20506, Malmö, Sweden
[6] Department of Radiotherapy, Shanghai Changhai Hospital, Second Military Medical University, Shanghai 200433, China
[7] Center for Applied Physics and Technology, Peking University, Beijing 100871, China
[8] Collaborative Innovation Center of IFSA (CICIFSA), Shanghai Jiao Tong University, Shanghai 200240, China
[9] The Third Institute of Surveying and Mapping of Hebei Province, Hebei Bureau of Geoinformation, Shijiazhuang 050000, China
Received 2016 June 21; revised 2016 August 24; accepted 2016 August 29; published 2016 October 12

ABSTRACT

Level energies, wavelengths, electric dipole, magnetic dipole, electric quadrupole, and magnetic quadrupole transition rates, oscillator strengths, and line strengths from combined relativistic configuration interaction and many-body perturbation calculations are reported for the 201 fine-structure states of the $2s^22p^6$, $2s^22p^53l$, $2s2p^63l$, $2s^22p^54l$, $2s2p^64l$, $2s^22p^55l$, and $2s^22p^56l$ configurations in all Ne-like ions between Cr XV and Kr XXVII. Calculated level energies and transition data are compared with experiments from the National Institute of Standards and Technology (NIST) and CHIANTI databases, and other recent benchmark calculations. The mean energy difference with the NIST experiments is only 0.05%. The present calculations significantly increase the amount of accurate spectroscopic data for the $n > 3$ states in a number of Ne-like ions of astrophysical interest. A complete data set should be helpful for analyzing new observations from solar and other astrophysical sources, and is also likely to be useful for modeling and diagnosing a variety of plasmas, including astronomical and fusion plasma.

Key words: atomic data – atomic processes

Supporting material: machine-readable tables

1. INTRODUCTION

The rapid advance of astronomical observations requires more extensive accurate spectroscopic data. This paper is a continuation of our recent work of providing the data of energy levels and transition characteristics for L-shell ions to the accuracy needed to exploit the high quality of observations from space-based and ground-based telescopes. Systematic calculations for the beryllium, carbon, and nitrogen isoelectronic sequences have already been performed (Wang et al. 2014, 2015, 2016). In this paper, we report accurate data for the neon isoelectronic sequence between Cr XV and Kr XXVII.

In view of a stable closed L-shell ground state, Ne-like ions show high abundance over a wide range of temperatures in ionization equilibrium (Mazzotta et al. 1998; Bryans et al. 2006, 2009; Liang & Badnell 2010). A wealth of emission lines in a wide wavelength range are frequently observed in astrophysics (Feldman et al. 2000; Behar et al. 2001; Mewe et al. 2001; Kaastra et al. 2002; Ko et al. 2002; Raassen et al. 2002; Ness et al. 2003; Curdt et al. 2004; Holczer et al. 2005; Landi & Phillips 2005; Brown et al. 2008; Del Zanna 2008; Shestov et al. 2008; Warren et al. 2008; Raassen & Pollock 2013; Del Zanna & Mason 2014; Shestov et al. 2014). These observations constitute an important tool for obtaining useful information of the physical conditions, chemical abundances, and evolution of the astrophysical objects. For example, in high-resolution observations with the *Chandra* and *XMM-Newton* X-ray observatories, the Fe XVII spectrum dominated the X-ray emission in the 700–1000 eV range of a large number of astrophysical objects. Thus these spectral lines were used for diagnostics (Paerels & Kahn 2003; Del Zanna 2011). The Fe XVII EUV lines were measured by the *Hinode* Imaging Spectrometer and provided useful information about the nature of the heating in the solar corona (Culhane et al. 2007; Del Zanna & Ishikawa 2009). The Ni XIX lines have been identified in the spectra of solar flares (Phillips et al. 1982; Landi & Phillips 2005), the Capella (Behar et al. 2001), and the supergiant star (Raassen & Pollock 2013), and offer an opportunity for determining elemental abundances and physical conditions of astrophysical objects.

Using various methods, a number of calculations have been carried out to provide data sets of energy structures and transition rates for the Ne-like sequence (Cogordan et al. 1985; Quinet et al. 1991; Hibbert et al. 1993; Dong et al. 2003a, 2003b; Froese Fischer & Tachiev 2004; Gu 2005b; Del Zanna & Ishikawa 2009; Ishikawa et al. 2009; Jönsson et al. 2014). However, in these studies the calculations were restricted to the $n \leqslant 3$ states (the 37 fine-structure states of the $(1s^2)2s^22p^6$, $2s^22p^53l$, and $2s2p^63l$ configurations).

Atomic data involving higher-lying states of the $n > 3$ configurations are also urgently demanded because of their wide applications for line identifications and plasma diagnostics in solar physics and astrophysics (Phillips et al. 1982; Acton et al. 1985; Del Zanna 2008; Del Zanna &

Ishikawa 2009; Raassen & Pollock 2013; Del Zanna & Mason 2014). Calculations were performed for the $n > 3$ states in Fe XVII using various methods, including the calculations of Chen et al. (2003) and Nahar et al. 2003 using the configuration interaction (CI) method of the code SUPERSTRUCTURE (Eissner et al. 1974), and the calculation by Aggarwal et al. (2004) utilizing the GRASP code of Dyall et al. (1989). Relativistic perturbation theory with a model potential was used to calculate the transition probabilities of the lowest 72 excited energy states to the ground state for ions up to $Z = 66$ (Ivanova & Gulov 1991). Using mixed CI and perturbation theory, energies and oscillator strengths for the seven lowest $J = 1$ odd excited states of neon-like ions with $Z = 11$–18 were calculated by Savukov (2003). Relativistic combined configuration interaction (RCI) and many-body perturbation theory (MBPT) calculations were carried out for wavelengths of $n \rightarrow 2$ ($3 \leqslant n \leqslant 7$) transitions in Fe XVII and Ni XIX (Gu 2007). Liang & Badnell (2010) reported the results for the energy levels, and transition data among the 209 states of the $2s^22p^6$, $(2s, 2p)^7nl$ ($n \leqslant 5$ and $l \leqslant n - 1$), and $2s^22p^5n'l'$ ($6 \leqslant n' \leqslant 7$ and $l' \leqslant 2$) configurations in Ne-like ions from Na II to Kr XXVII using the AUTOSTRUCTURE code (Badnell 1986). Among the above $n > 3$ calculations, the MBPT results of Gu (2007) in Fe XVII and Ni XIX are sufficiently accurate to identify observed spectra. In this work, however, transition properties were not computed. The other mentioned calculations are not adequate to meet the accuracy requirements of line identification and interpretation in astrophysics.

The present work aims at extending the accurate calculations for Fe XVII and Ni XIX by Gu (2007), providing the energy data of spectroscopic accuracy and transition rates for the $n \leqslant 6$ states in a number of Ne-like ions of astrophysical interest. By using a combined RCI and MBPT approach in FAC (Gu 2003, 2005a, 2005b; Gu et al. 2006), we present data for the lowest 201 bound energy states arising from the $2s^22p^6$, $(2s, 2p)^7nl$ ($3 \leqslant n \leqslant 4$ and $l \leqslant n - 1$), and $2s^22p^5n'l'$ ($5 \leqslant n' \leqslant 6$ and $l' \leqslant n' - 1$) configurations in Ne-like ions from Cr XV to Kr XXVII, as well as the electric dipole (E1), electric quadrupole (E2), magnetic dipole (M1), and magnetic quadrupole (M2) transition rates among these states. To assess the accuracy of the MBPT data, the multiconfiguration Dirac–Hartree–Fock (MCDHF) and RCI method implemented in GRASP2K (Jönsson et al. 2007, 2013) has been used to calculate the data for Fe XVII (hereafter referred to as MCDHF/RCI). The MBPT energies in Fe XVII agree well with the MCDHF/RCI values, as well as the experimental energies from the Atomic Spectra Database (ASD) of the National Institute of Standards and Technology (NIST) (Kramida et al. 2015). The energy differences between the calculated MBPT and MCDHF/RCI level energies are within 0.07% for all 201 states in Fe XVII, and the mean difference of the NIST and MBPT values is 0.05% for the 425 states listed in the NIST ASD. Compared with the recent systematic MCDHF and RCI calculations by Jönsson et al. (2014), in which both accurate energy levels and transition rates were given, the present calculations are extended to report the data for additional 174 levels of the $2s2p^63l$, $2s^22p^54l$, $2s2p^64l$, $2s^22p^55l$, and $2s^22p^56l$ configurations. The calculations also extend the elaborate work by Gu (2005b, 2007) to include data of an additional 11 neon-like ions between Cr XV and Kr XXVII. The excellent description of the energy separations along the sequence makes it possible to point out a number of lines for which the experimental identifications can be questioned. A complete data set including energy levels and transition data should be helpful for analyzing new data from solar and other astrophysical sources.

2. THEORY

2.1. The MBPT Method

According to Rayleigh–Schrödinger perturbation theory, the no-pair Dirac–Coulomb–Breit (DCB) Hamiltonian $H_{\rm DCB}$ for an N-electron ionic system can be written as (Sucher 1980; Gu 2005a, 2005b):

$$H_{\rm DCB} = \sum_i^N \left[h_d(i) - \frac{Z}{r_i} \right] + \sum_{i<j}^N \left(\frac{1}{r_{ij}} + B_{ij} \right), \quad (1)$$

where $h_d(i)$ and Z are the free-electron Dirac Hamiltonian and the nuclear charge, respectively. r_i and r_{ij} are the radial coordinate of electron i, and the distance between the electrons i and j, respectively. B_{ij} is the frequency-independent Breit interaction given by

$$B_{ij} = -\frac{1}{2r_{ij}} \left[\boldsymbol{\alpha}_i \cdot \boldsymbol{\alpha}_j + \frac{(\boldsymbol{\alpha}_i \cdot \boldsymbol{r}_{ij})(\boldsymbol{\alpha}_j \cdot \boldsymbol{r}_{ij})}{r_{ij}^2} \right]. \quad (2)$$

where $\boldsymbol{\alpha}_i$ is a matrix vector constructed from Pauli spin matrices. $H_{\rm DCB}$ is divided into two parts, namely, a model Hamiltonian H_0 and a perturbation V, given by

$$H_0 = \sum_i [h_d(i) + U(r_i)], \quad (3)$$

$$V = -\sum_i \left[\frac{Z}{r_i} + U(r_i) \right] + \sum_{i<j} \left(\frac{1}{r_{ij}} + B_{ij} \right), \quad (4)$$

where $U(r)$ is a model potential including the screening effects of all electrons, whose appropriate choice makes V as small as possible.

For calculations:

(a) The approximated local central potential $U(r)$ and eigenfunctions Φ_k of H_0 are obtained by the Dirac–Fock–Slater self-consistent field calculations.
(b) The Hilbert space of the Hamiltonian is divided into two parts, namely a model space M, and the orthogonal space O. A subset of Φ_k will define the space M, and the remaining states belong to the space O.
(c) The second-order eigenvalues are obtained through solving the generalized eigenvalue problem for the first-order effective Hamiltonian.

2.2. The MCDHF Method

The MCDHF method was described in detail by Grant (2007), and here we just give a brief outline. The atomic state function is given as an expansion over configuration state functions (CSFs)

$$\Psi(\gamma J\pi) = \sum_j c_j \Phi(\gamma_j J\pi), \quad (5)$$

where J and π are the total angular momentum and parity of the system, respectively, γ_j is a set of quantum numbers, in

Table 1
Level Energies (in eV) of the States in Ne-like Ions from Cr XV to Kr XXVII, and Level Designations in Both the LSJ- and *jj* Coupling Schemes, and the Dominant Mixing Coefficients of the LSJ Basis

Z	Key	Conf	LSJ	jj[a,b,c]	J^π	Energy		Mixing Coefficients LSJ[f]
						NIST[d]	MBPT[e]	
26	1	$2s^22p^6$	$^1S_0$	$2p + 4(0)0$	0^e	0.000000E+00	0.000000E+00	−1.00(1)
26	2	$2s^22p^53s$	$^3P_2$	$2p + 3(3)3\ 3s + 1(1)4$	2^o	7.249150E+02	7.252443E+02	−1.00(2)
26	3	$2s^22p^53s$	$^1P_1$	$2p + 3(3)3\ 3s + 1(1)2$	1^o	7.267839E+02	7.271388E+02	−0.74(3) − 0.67(5)
26	4	$2s^22p^53s$	$^3P_0$	$2p - 1(1)1\ 3s + 1(1)0$	0^o	7.375376E+02	7.378560E+02	−1.00(4)
26	5	$2s^22p^53s$	$^3P_1$	$2p - 1(1)1\ 3s + 1(1)2$	1^o	7.387243E+02	7.390537E+02	−0.74(5)0.67(3)
26	6	$2s^22p^53p$	$^3S_1$	$2p + 3(3)3\ 3p - 1(1)2$	1^e	7.552334E+02	7.554915E+02	−0.90(6)0.42(13)
26	7	$2s^22p^53p$	$^3D_2$	$2p + 3(3)3\ 3p - 1(1)4$	2^e	7.586933E+02	7.589928E+02	−0.76(7) − 0.55(14)
26	8	$2s^22p^53p$	$^3D_3$	$2p + 3(3)3\ 3p + 1(3)6$	3^e	7.603239E+02	7.606096E+02	1.00(8)
26	9	$2s^22p^53p$	$^1P_1$	$2p + 3(3)3\ 3p + 1(3)2$	1^e	7.614395E+02	7.617403E+02	−0.71(9)0.50(12) − 0.44(13)
26	10	$2s^22p^53p$	$^3P_2$	$2p + 3(3)3\ 3p + 1(3)4$	2^e	7.632480E+02	7.635530E+02	−0.82(10) − 0.57(14)

Notes. Only the lowest 10 levels in Ne-like Fe are shown here.
[a] The number at the end or inside of the bracket is $2J$.
[b] $s + = s_{1/2}$, $p- = p_{1/2}$, $p + = p_{3/2}$, $d- = d_{3/2}$, $d + = d_{5/2}$, $f- = f_{5/2}$, $f + = f_{7/2}$, $g- = g_{7/2}$, $g + = g_{9/2}$, $h- = h_{9/2}$, and $h + = h_{11/2}$.
[c] The number after ± is the occupation number of the corresponding sub-shell. For example, the *jj* configuration of level 2 is $2s^2_{1/2}2p^2_{1/2}2p^3_{3/2}3s_{1/2}$.
[d] The observed energies from the NIST ASD (Kramida et al. 2015).
[e] The present MBPT results.
[f] The mixing coefficient of the LSJ basis of the state indicated by the key in parenthesis.

(This table is available in its entirety in machine-readable form.)

Table 2
Wavelengths(λ, in Å), Line Strengths(S, in Atomic Units), Weighted Oscillator Strengths (gf, Dimensionless) and Transition Rates(A, in s^{-1}) for the Transitions in Ne-Like Ions from Cr XV to Kr XXVII

Z	$j - i$	Type	λ	S	gf	A
26	2 − 1	M2	1.7103E+01	1.013E−01	4.525E−08	2.063E+05
26	3 − 1	E1	1.7059E+01	6.862E−03	1.222E−01	9.335E+11
26	3 − 2	M1	6.6341E+03	1.118E+00	6.816E−07	3.443E+01
26	4 − 3	M1	1.1529E+03	8.879E−01	3.114E−06	1.563E+04
26	5 − 1	E1	1.6784E+01	5.518E−03	9.986E−02	7.882E+11
26	5 − 2	M1	8.9783E+02	1.347E+00	6.069E−06	1.674E+04
26	5 − 3	M1	1.0384E+03	3.670E−01	1.429E−06	2.948E+03
26	5 − 4	M1	1.0448E+04	1.089E+00	4.214E−07	8.582E+00

Note. Only transitions among the lowest five states in Fe XVII are shown here.

(This table is available in its entirety in machine-readable form.)

addition to $J\pi$, to specify a CSF, and c_j is the mixing coefficient.

For calculations:

(a) A CSF $\Phi(\gamma_j J\pi)$ is constructed from a product of single-electron wavefunctions through a proper angular momentum coupling and antisymmetrization.
(b) The self-consistent iteration method is used to simultaneously obtain the Dirac orbitals and the expansion coefficients.
(c) When the radial orbitals are obtained, RCI calculations are performed, which include the Breit interaction and first-order Quantum Electrodynamics (QED) corrections (self-energy and vacuum polarization).

3. CALCULATIONS AND RESULTS

In the MBPT calculations, the model space M contains the configurations $2s^22p^6$, $(2s, 2p)^7nl$ ($3 \leqslant n \leqslant 4$ and $l \leqslant n - 1$), and $2s^22p^5n'l'$ ($5 \leqslant n' \leqslant 6$ and $l' \leqslant n' - 1$). The N space contains all configurations formed by single and double (SD) virtual excitations of the M space. For single/double excitations, configurations with $n \leqslant 200$ and $l \leqslant \min(n - 1, 25)$/the inner electron promotion up to $n = 65$ and promotion of the outer electron up to $n' = 200$ are considered. For level energy and radiative transition calculations, some corrections such as finite nuclear size, nuclear recoil, and QED are also included. A more detailed description of the MBPT calculation procedure can be found in our recent work (Wang et al. 2014, 2015, 2016).

Table 1 displays the computed excitation energies of 201 fine-structure levels in Ne-like ions (Z = 24–36) obtained from the MBPT method. Also listed in the table are the experimental energy levels recommended by the NIST ASD. Among the 2613 energy levels in the 13 ions given by the MBPT method, 443 experimental results are available. The wavelengths (λ_{ji} in Å), line strengths (S_{ji} in atomic units, 1 au = 6.460×10^{-36} cm^2 esu^2), weighted oscillator strengths (gf_{ji} dimensionless) and radiative rates (A_{ji} in s^{-1}) for the E1, M1, E2, and M2 transitions among the 201 levels for each ion, are listed in Table 2.

Table 3
Comparisons of the Experimental and Theoretical Energies in Fe XVII

Key	Config.	LSJ	Energy					
			Exp.		Cal.			
			NIST[a]	CHAINTI[b]	MBPT[c]	MCDHF/RCI[d]	MCDHF/RCI2[e]	MR-MP[f]
1	$2s^22p^6$	$^1S_0$	0.0000	0.000	0.0000	0.0000	0.0000	0.0000
2	$2s^22p^53s$	$^3P_2$	725.2443	725.223	724.9150	725.1672	725.1969	725.170
3	$2s^22p^53s$	$^1P_1$	727.1388	727.138	726.7839	727.0773	727.1015	727.060
4	$2s^22p^53s$	$^3P_0$	737.8560	737.889	737.5376	737.8046	737.8303	737.815
5	$2s^22p^53s$	$^3P_1$	739.0537	739.073	738.7243	739.0032	739.0243	738.997
6	$2s^22p^53p$	$^3S_1$	755.4915	755.485	755.2334	755.2505	755.5067	755.462
7	$2s^22p^53p$	$^3D_2$	758.9928	758.980	758.6933	758.7627	759.0026	758.939
8	$2s^22p^53p$	$^3D_3$	760.6096	760.599	760.3239	760.3758	760.6175	760.564
9	$2s^22p^53p$	$^1P_1$	761.7403	761.746	761.4395	761.5072	761.7462	761.688
10	$2s^22p^53p$	$^3P_2$	763.5530	763.550	763.2480	763.3194	763.5543	763.496

Notes. Only the lowest 10 levels in Ne-like Fe are shown here.
[a] The observed energies from the NIST ASD (Kramida et al. 2015).
[b] The observed energies from the Chianti database (Dere et al. 1997; Del Zanna et al. 2015).
[c] The present MBPT energies.
[d] The present MCDHF/RCI energies.
[e] The MCDHF/RCI2 energies calculated by Jönsson et al. (2014).
[f] The MR-MP energies calculated by Ishikawa et al. (2009).
(This table is available in its entirety in machine-readable form.)

To assess the accuracy of the MBPT results, the MCDHF and subsequent RCI calculations are carried out for Fe XVII. Separate calculations are performed for the even and odd states belonging to the M space of the above MBPT calculations, which are considered as the multi-reference configurations. The CSFs' expansions are obtained through single and double excitations of the orbitals in the multi-reference configurations with orbitals in an active set with principal quantum numbers $n = 3, \ldots, 8$ and angular symmetries s, p, d, f, g, h, and i. To monitor the convergence of the calculated energies and transition parameters, the active sets were increased in a systematic way by adding layers of orbitals. For the $n = 8$ expansion this resulted in 3034729 CSFs with even parity and 3009779 CSFs with odd parity. The self-consistent field calculations for each layer of orbitals are followed by RCI calculations. A more detailed description of the MCDHF/RCI calculation procedure can be found in our recent work (Jönsson et al. 2013, 2014; Si et al. 2015a, 2015b).

4. EVALUATION OF DATA

4.1. Energy Levels

Regarding experimental data and elaborate computed results along the isoelectronic sequence, the Fe XVII spectrum is currently the most studied spectrum in astrophysics. For example, many Fe XVII EUV lines observed by the Hinode EUV Imaging Spectrometer were identified by Del Zanna & Ishikawa (2009). These Fe XVII lines provide useful information about the nature of the heating in the solar corona. In Table 3, the MBPT energy results for the 201 levels in Fe XVII are compared with the experimental values of Del Zanna & Ishikawa (2009), who reviewed the Fe XVII spectrum in the 30–450 Å range, and provided accurate results for the $n = 3$–5 states, which have been included in CHIANTI (Dere et al. 1997; Del Zanna et al. 2015). The present MCDHF/RCI values, the previous results for the $2s^22p^6$ and $2s^22p^53l$ levels (Jönsson et al. 2014, MCDHF/RCI2), and the relativistic multi-reference Möller–Plesset results for the $2s^22p^6$ and $2l^73l'$ states (Ishikawa et al. 2009, MR-MP), as well as the experimental values from the NIST ASD, are also given in the table for comparison. Compared with the present MBPT calculations, Gu (2005b) adopted the same method, and reported similar results that are not shown in this table.

Compared with the previous elaborate computed results (MCHDF/RCI2 and MR-MP) for the $n = 3$ levels, the present MBPT and MCDHF/RCI calculations give very consistent results. The experimental values from the NIST and CHIANTI databases and the four theoretical data sets also show good agreement (within 0.1%) for the $n = 3$ states, except for the $2s2p^63s$ $^1S_0$ state. For this level, the NIST value 869.1 eV is observed at a considerably higher energy (about 4 eV) than the CHIANTI experimental value 865.266 eV and the MBPT, MCHDF/RCI and MR-MP theoretical values (864.8332, 865.2301 and 865.146 eV).

Observed energies are scarce and the identification of some states becomes questionable for the $n > 3$ states. The $2s^22p^54d$ $^1D_2$ (1010.682 eV), and $2s^22p^54f$ $^1G_4$ (1017.9 eV) and $2s^22p^54f$ $^3G_4$ (1014.2 eV) states in the NIST ASD do not have any obvious counterparts in the Chianti database or in calculated energies, and misidentification cannot be ruled out. As an example, we analyze the $2s^22p^54f$ $^1G_4$ (1017.9 eV) state in more detail. By means of the $2s^22p^53d$ $^3D_3$ level energy, the observed wavelength 58.98 Å ($2s^22p^53d$ $^3D_3$–$2s^22p^54f$ $^1G_4$) is utilized to extract the $2s^22p^54f$ $^1G_4$ level energy (Shirai et al. 2000). This NIST wavelength is about 1.4% lower than the CHIANTI, MBPT, and MCDHF/RCI values (59.776, 59.821, and 58.856 Å), but is very close to the CHIANTI, MBPT, and MCDHF/RCI values (58.980, 58.026, and 59.057 Å) for the $2s^22p^53d$ $^3F_3$–$2s^22p^54f$ $^1G_4$ transition, whose the lower state is $2s^22p^53d$ $^3F_3$, but not $2s^22p^53d$ $^3D_3$. And the transition rate is 1.075×10^{12} s^{-1} for the $2s^22p^53d$ $^3F_3$–$2s^22p^54f$ $^1G_4$ ($\Delta L = 1$) transition, which is indeed larger by over one order of magnitude than

Table 4
Level Energies (in eV) for the States in which the NIST Experimental Values Differ from the MBPT Results by More than 0.2%

Z	Key[a]	State	Energy		Difference (%)
			MBPT[b]	NIST[c]	
24	29	$2s2p^63s\ ^1S_0$	707.2378	712.822	−0.78
24	87	$2s^22p^55d\ ^3P_1$	884.1274	886.24	−0.24
26	29	$2s2p^63s\ ^1S_0$	864.8332	869.1	−0.49
26	57	$2s^22p^54d\ ^1D_2$	1007.727	1010.682	−0.29
26	67	$2s^22p^54f\ ^3F_4$	1015.338	1017.9	−0.25
26	73	$2s^22p^54f\ ^3G_4$	1027.657	1014.2	1.33
28	28	$2s2p^63s\ ^3S_1$	1031.886	1036.26	−0.42
28	29	$2s2p^63s\ ^1S_0$	1038.504	1043.45	−0.47
30	27	$2s^22p^53d\ ^1P_1$	1185.086	1188.26	−0.27
31	97	$2s2p^64p\ ^1P_1$	1742.279	1768.63	−1.49
32	87	$2s2p^64p\ ^3P_1$	1878.827	1883.07	−0.23
32	89	$2s2p^64p\ ^1P_1$	1882.237	1886.79	−0.24
34	47	$2s^22p^54s\ ^3P_1$	1986.773	1961.1820	1.30
35	71	$2s^22p^54d\ ^3D_1$	2189.996	2194.7682	−0.22
35	83	$2s2p^64p\ ^1P_1$	2337.637	2342.8053	−0.22
35	97	$2s^22p^55d\ ^1P_1$	2355.808	2361.1550	−0.23
35	131	$2s^22p^55d\ ^3D_1$	2402.879	2408.3929	−0.23
35	155	$2s^22p^56d\ ^1P_1$	2470.301	2477.2042	−0.28

Notes.
[a] The index number of the level given in Table 1.
[b] The present MBPT energies.
[c] The NIST recommended energies (Kramida et al. 2015).

the 8.8×10^{10} s^{-1} for the $2s^22p^53d\ ^3D_3$–$2s^22p^54f\ ^1G_4$ ($\Delta L = 2$) transition. Therefore, we conclude that the $\Delta L = 1$ transition is more likely to be observed than the $\Delta L = 2$ transition, and the NIST wavelength 58.98 Å should be assigned to the $2s^22p^53d\ ^3F_3$–$2s^22p^54f\ ^1G_4$ transition. By means of this wavelength and the NIST energy 805.0331 eV of the $2s^22p^53d\ ^3F_3$ states, the NIST value for $2s^22p^54f\ ^1G_4$ should be changed to 1015.3 eV, which agrees with the CHIANTI, MBPT, and MCDHF/RCI (1015.96, 1015.255, and 1015.461 eV) to within 0.1%. Based on the above argument, a misidentification for this NIST level cannot be ruled out. Together with the $2s^22p^54f\ ^1G_4$ (1017.9 eV) energy, all the other NIST values for the $2s2p^63s\ ^1S_0$, $2s^22p^54d\ ^1D_2$, and $2s^22p^54f\ ^3G_4$ states in Fe XVII, for which the NIST results differ from the MBPT values by more than 0.2%, are tabulated in Table 4.

The agreement of the CHIANTI experimental energies and the MBPT results is better. Deviations are less than 0.2% for all 30 $n = 4, 5$ states listed in the CHIANTI database, and are within 0.1% for 28 states. We can also see from Table 3 that the present MBPT and MCDHF/RCI calculations give very consistent results for all the 201 $n \leqslant 6$ levels, and the deviation of the two data sets is within 0.07% for all levels. The calculations predict energy levels with such a high precision that the results can be utilized to analyze the new observations from space-based and ground-based telescopes.

To further assess the accuracy of the MBPT energies, we compare them with the NIST experimental values for all the 13 Ne-like ions. Among the 2613 energy levels in 13 ions given by the MBPT method, the 443 NIST results are available. The computed energies agree very well with the NIST values. The differences between experimental and calculated energies are less than 0.1% for 393 states, and are within 0.2% for another

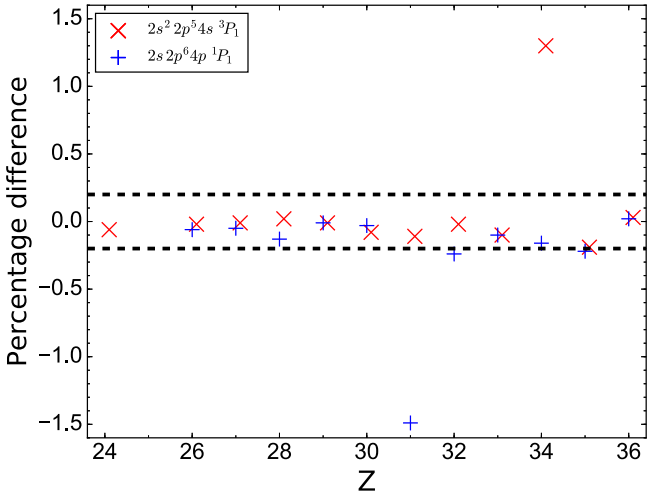

Figure 1. Percentage differences of the MBPT energies relative to the NIST observations for the $2s^22p^54s\ ^3P_1$ and $2s2p^64p\ ^1P_1$ states along the sequence.

32 states. The remaining 18 states including four levels in Fe XVII discussed in detail above, for which the deviations are larger than 0.2%, are listed in Table 4. We cannot find any obvious duplicate energies in the present MBPT calculations, and these NIST values should be carefully used. As an example, Figure 1 shows the energy deviations as functions of Z for the $2s^22p^54s\ ^3P_1$ and $2s2p^64p\ ^1P_1$ states. Some obvious anomalies are seen for the $2s^22p^54s\ ^3P_1$ state in Se XXV (the difference is about 1.3%), and the $2s2p^64p\ ^1P_1$ state (1.5%) in Ga XXII. The differences fall between 0.2% and 0.3% for the $2s2p^64p\ ^1P_1$ state in Ge XXIII and Br XXVI. The misidentification, line blending, or large experimental errors of the spectral observations could be responsible for the large uncertainty of the data compiled by the NIST ASD (Kramida et al. 2015). Apart from these irregularities, the two data sets agree well for most states along the sequence.

In short, apart from the 18 states included in Table 4, the mean energy deviation of the observed and computed values for the 425 states included in the NIST ASD is 0.05%. Seeing that the same computational procedure is adopted for each ion, which implies that the quality of the data should be consistent and systematic, we conclude that relatively large uncertainties of observed energies bring on the large deviations for these states, and these NIST values should be re-evaluated.

4.2. Radiative Rates

In Table 5, weighted oscillator strengths for the E1, M1, E2, and M2 transitions among the $n \leqslant 3$ levels of the $2s^22p^6$, $2s^22p^53s$, $3p$, and $3d$, and $2s2p^63s$, $3p$ and $3d$ configurations are shown. Our results, gf(MBPT) and gf(MCDHF/RCI), are compared for Fe XVII with the calculated values from Jönsson et al. (2014), gf(MCDHF/RCI2), and the NIST ASD (Kramida et al. 2015), gf(NIST). The overall agreement among the present MBPT and MCDHF/RCI values and the previous MCDHF/RC2 results is good, and the relative deviations are within 10% for most of the transitions. The average differences (with standard deviations) are 3.1% ± 4.4% between the MBPT and MCDHF/RCI values and 2.1% ± 3.1% between the MBPT and MCDHF/RCI2 values, which are also satisfactory. Among the large number of the transitions listed in Table 5, the gf values for some transitions (20 transitions) are

Table 5
Comparisons of the Oscillator Strengths (gf) for the Transitions among the $n \leqslant 3$ Levels in Fe XVII

$j-i$	Transition	Type	gf			
			MBPT[a]	MCDHF/RCI[b]	MCDHF/RCI2[c]	NIST[d]
2 − 1	$2s^22p^53s\ ^3P_2 - 2s^22p^6\ ^1S_0$	M2	4.525E−08	4.599E−08	4.559E−08	…
3 − 1	$2s^22p^53s\ ^1P_1 - 2s^22p^6\ ^1S_0$	E1	1.222E−01	1.232E−01	1.219E−01	1.22E−01
5 − 1	$2s^22p^53s\ ^3P_1 - 2s^22p^6\ ^1S_0$	E1	9.986E−02	1.028E−01	1.013E−01	1.05E−01
7 − 1	$2s^22p^53p\ ^3D_2 - 2s^22p^6\ ^1S_0$	E2	1.019E−04	1.023E−04	1.023E−04	…
10 − 1	$2s^22p^53p\ ^3P_2 - 2s^22p^6\ ^1S_0$	E2	1.074E−04	1.087E−04	1.085E−04	…
14 − 1	$2s^22p^53p\ ^1D_2 - 2s^22p^6\ ^1S_0$	E2	1.253E−04	1.270E−04	1.267E−04	…
17 − 1	$2s^22p^53d\ ^3P_1 - 2s^22p^6\ ^1S_0$	E1	9.718E−03	1.018E−02	9.864E−03	9.70E−03
18 − 1	$2s^22p^53d\ ^3P_2 - 2s^22p^6\ ^1S_0$	M2	1.102E−06	1.120E−06	1.109E−06	…
21 − 1	$2s^22p^53d\ ^1D_2 - 2s^22p^6\ ^1S_0$	M2	1.931E−07	1.978E−07	1.961E−07	…
23 − 1	$2s^22p^53d\ ^3D_1 - 2s^22p^6\ ^1S_0$	E1	6.379E−01	6.456E−01	6.367E−01	6.30E−01
24 − 1	$2s^22p^53d\ ^3F_2 - 2s^22p^6\ ^1S_0$	M2	6.616E−08	6.892E−08	6.816E−08	…
25 − 1	$2s^22p^53d\ ^3D_2 - 2s^22p^6\ ^1S_0$	M2	5.864E−08	5.773E−08	5.761E−08	…
27 − 1	$2s^22p^53d\ ^1P_1 - 2s^22p^6\ ^1S_0$	E1	2.220E+00	2.288E+00	2.269E+00	2.31E+00
31 − 1	$2s2p^63p\ ^3P_1 - 2s^22p^6\ ^1S_0$	E1	3.674E−02	3.589E−02	…	3.00E−02
32 − 1	$2s2p^63p\ ^3P_2 - 2s^22p^6\ ^1S_0$	M2	1.199E−07	1.208E−07	…	…
33 − 1	$2s2p^63p\ ^1P_1 - 2s^22p^6\ ^1S_0$	E1	2.865E−01	2.905E−01	…	2.80E−01
37 − 1	$2s2p^63d\ ^1D_2 - 2s^22p^6\ ^1S_0$	E2	1.390E−03	1.398E−03	…	…

Notes. The MBPT and MCDHF/RCI values, as well as the MCDHF/RCI2 and NIST Results, are listed for comparison. Only transitions involving the ground state in Ne-like Fe are shown here.
[a] The present MBPT oscillator strengths.
[b] The present MCDHF/RCI oscillator strengths.
[c] The MCDHF/RCI oscillator strengths given by Jönsson et al. (2014).
[d] The oscillator strengths recommended by the NIST ASD.

(This table is available in its entirety in machine-readable form.)

given by the NIST ASD. The NIST gf values for these 20 transitions are compared with the MBPT gf values in Figure 2(a). The two data sets agree within 10% for 13 transitions, while differing from each other between 10% and 35% for the 7 transitions. Note that good agreement (within 6%) can be found between the MBPT and MCDHF/RCI gf values for all transitions in Figure 2(a), and thus the NIST values for these seven transitions, which are compiled by Fuhr et al. (1988), should be updated.

Weighted oscillator strengths among the $n \leqslant 3$ states in Fe XVII given by the CHIANTI database are also compared with the present MBPT gf values in Figure 2(b). Many of the CHIANTI compilations differ from the present calculations by 10%–50%, and moreover, the deviations exceed 10% for many relatively strong transitions with gf values $\geqslant 10^{-2}$. The agreement of the present two calculations is within 10% for all strong transitions, and is no more than 15% for a few weak transitions.

To further assess the accuracy of the present calculations, in Figure 3 the MCDHF/RCI weighted oscillator strengths are compared with the MBPT values for all the 1557 strong transitions ($gf \geqslant 10^{-2}$) among the $n \leqslant 6$ states in Fe XVII, and the comparison of the MBPT and MCDHF/RCI2 calculations for all 675 strong transitions among the $n \leqslant 3$ states from Cr XV to Kr XXVII are shown in Figure 4. For 92% of the transitions in Fe XVII shown in Figure 3, the agreement of the present two calculations is within 10%, while they differ from each other by over 20% (but less than 40%) for only 29 transitions. The upper states of these 29 transitions mostly belong to the highest states of the $n = 6$ configurations. For such transitions, the present MCDHF/RCI calculations converge very slowly with increasing active sets. Nevertheless, the

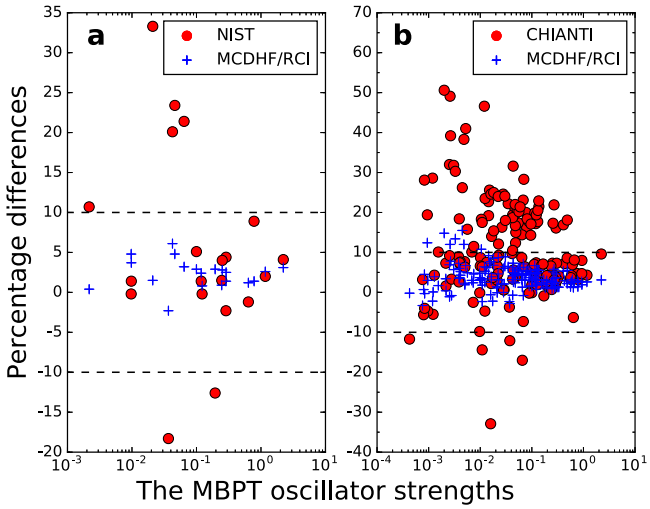

Figure 2. (a) Percentage differences of the NIST and MCDHF/RCI oscillator strengths relative to the present MBPT results for the transitions among the $n \leqslant 3$ states given by the NIST ASD. (b) Percentage differences of the CHIANTI and MCDHF/RCI oscillator strengths relative to the present MBPT results for the transitions among the $n \leqslant 3$ states given by the CHIANTI database. Dashed lines indicate differences of ±10%.

average difference with the standard deviation of the present two calculations for the 1557 transitions is only 3.0% ± 5.5%. In addition, as shown in Figure 4 the MBPT and MCDHF/RCI2 gf values for the 675 transitions among the $n \leqslant 3$ states from Cr XV to Kr XXVII agree within 10% for 672 transitions. The average difference with the standard deviation of the two calculations for all transitions is only 1.4% ± 1.2%, which is highly satisfactory.

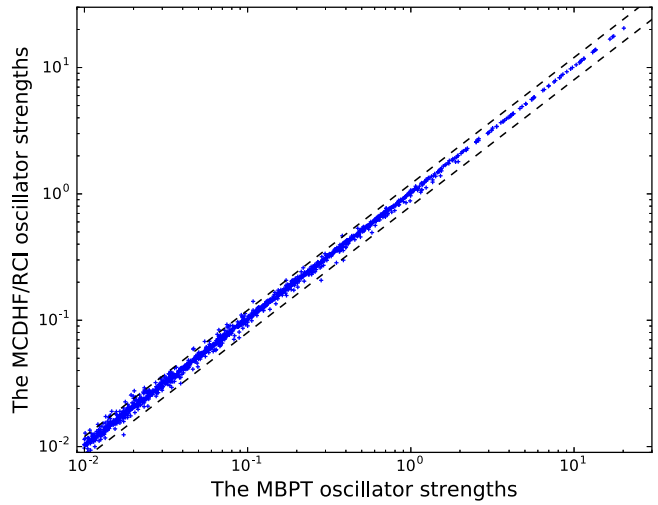

Figure 3. Comparison of the present MBPT oscillator strengths with the MCDHF/RCI results for the transitions with $gf \geqslant 0.01$ in Fe XVII. The dashed lines indicate differences of ±20%.

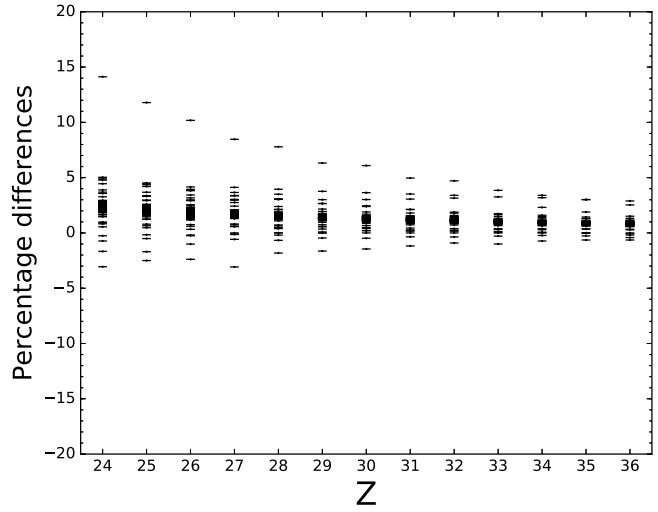

Figure 4. Comparison between the MCDHF/RCI2 and MBPT oscillator strengths for the $gf \geqslant 0.01$ transitions among the $n \leqslant 3$ states along the sequence.

Based on the above analysis we conclude that the present transition data have better accuracy compared to the values from the NIST and CHIANTI databases. Using the part of the transition values with insufficient accuracy, especially for the strong transitions, may lead to quite different, even wrong results when carrying out line identifications and plasma diagnostics in solar physics and astrophysics. Therefore, hopefully it would be possible to replace the existing CHIANTI data, as well as the NIST values, with the present MBPT and/or MCDHF/RCI results.

Del Zanna (2011) have pointed out that the Fe XVII lines in the X-ray range can be reliably used for the measurement of electron temperatures in the solar corona and other astrophysical sources. Using the MBPT radiative transition data, as well as the collisional atomic data recommended by the CHIANTI database, in conjunction with the statistical equilibrium code of Dufton (1977), the synthetic Fe XVII spectra in the range of 10–20 Å are shown in Figure 5. The intensity of each transition is represented by a Gaussian distribution with a resolving power of 1000, corresponding to a temperature

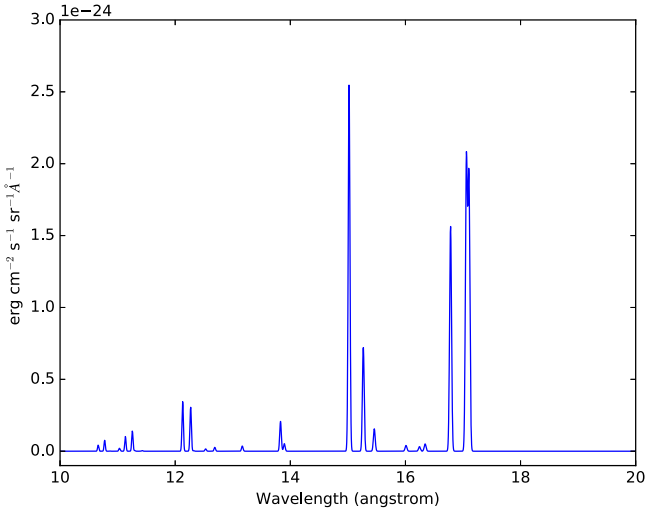

Figure 5. Synthetic Fe XVII spectrum containing transitions between 10 and 20 Å. See the text for details.

$T_e = 10^7$ K and a density $N_e = 10^{11}$ cm^{-3} , a typical solar flare condition. As shown in Figure 5, prominent transitions (with wavelengths and transition rates) in the 10–20 Å range are

$2s^22p^6\ {}^1S_0 - 2s^22p^55d\ {}^1P_1$ (11.256 Å and 3.07×10^{12} s^{-1})
$2s^22p^6\ {}^1S_0 - 2s^22p^54d\ {}^1P_1$ (12.130 Å and 5.62×10^{12} s^{-1})
$2s^22p^6\ {}^1S_0 - 2s^22p^54d\ {}^3D_1$ (12.269 Å and 5.08×10^{12} s^{-1})
$2s^22p^6\ {}^1S_0 - 2s2p^63p\ {}^1P_1$ (13.830 Å and 3.33×10^{12} s^{-1})
$2s^22p^6\ {}^1S_0 - 2s^22p^53d\ {}^3D_1$ (15.268 Å and 6.08×10^{12} s^{-1})
$2s^22p^6\ {}^1S_0 - 2s^22p^53d\ {}^3P_1$ (15.459 Å and 9.04×10^{10} s^{-1})
$2s^22p^6\ {}^1S_0 - 2s^22p^53s\ {}^3P_1$ (16.784 Å and 7.88×10^{11} s^{-1})
$2s^22p^6\ {}^1S_0 - 2s^22p^53s\ {}^1P_1$ (17.059 Å and 9.34×10^{11} s^{-1})
$2s^22p^6\ {}^1S_0 - 2s^22p^53s\ {}^3P_2$ (17.103 Å and 2.06×10^5 s^{-1})

The strongest resonance transition in the spectrum is $2s^22p^6\ {}^1S_0 - 2s^22p^53d\ {}^1P_1$ (15.021 Å and 2.19×10^{13} s^{-1}).

5. SUMMARY

Systematic and consistent MBPT calculations have been performed for Ne-like ions with $Z = 24 - 36$ using the FAC code. A complete data set with high accuracy, including energies, wavelengths, line strengths, oscillator strengths, and transition rates for the E1, M1, E2, and M2 transitions among the 201 states of the $2s^22p^6$, $(2s, 2p)^73l$, $(2s, 2p)^74l$, $2s^22p^55l$, and $2s^22p^56l$ configurations, has been deduced for each ion. The MBPT energy results are in excellent agreement with observations, and the mean energy deviation with the NIST observations is 0.05%. Compared with the elaborate MCDHF/RCI and MCDHF/RCI2 calculations, the accuracy of the MBPT transition data has been estimated to only 1.4% for transitions among the $n \leqslant 3$ states for all 13 ions, and 3.0% for transitions involving the higher states in Fe XVII. Because our calculations are systematic and consistent, reporting a unified quality of data, we expect that the transition rates are highly accurate and may serve as benchmarks for other calculations.

The present calculations significantly increase the amount of accurate energy data for a number of Ne-like ions of astrophysical interest, as well as their highly accurate transition rates. A re-analysis of electron temperature and density in solar or other astrophysical sources using the current extended data,

set to high accuracy, allows for a more thorough consistency check, with the possibility of identifying and including new lines of diagnostic value. Through this comparison, we can point out some observations that may have large errors or that were wrongly assigned, which have been included in Table 1. The high accuracy of the current data may rule out the possibility that wrongly identified lines enter the analysis.

The authors express their gratitude to Dr. MingFeng Gu for offering guidance in using his FAC code. We acknowledge the support from the National Natural Science Foundation of China (grants No. 11674066, No. 21503066, No. 11504421, and No. 11474034) and the support from the Foundation for the Development of Science and Technology of the Chinese Academy of Engineering Physics (grant No. 2012B0102012). This work is also supported by NSAF under Grant No. 11076009, the Chinese Association of Atomic and Molecular Data, the Chinese National Fusion Project for ITER No. 2015GB117000, and the Swedish Research Council under contract 2015-04842. One of the authors (K.W.) expresses his gratitude for the support from the visiting researcher program at Fudan University.

Software: FAC (Gu 2003, 2005a, 2005b; Gu et al. 2006), GRASP2K (Jönsson et al. 2007, 2013), CHIANTI (Dere et al. 1997; Del Zanna et al. 2015).

REFERENCES

Acton, L. W., Bruner, M. E., Brown, W. A., et al. 1985, ApJ, 291, 865
Aggarwal, K. M., Keenan, F. P., & Kisielius, R. 2004, A&A, 420, 783
Badnell, N. R. 1986, JPhB, 19, 3827
Behar, E., Cottam, J., & Kahn, S. M. 2001, ApJ, 548, 966
Brown, C. M., Feldman, U., Seely, J. F., Korendyke, C. M., & Hara, H. 2008, ApJS, 176, 511
Bryans, P., Badnell, N. R., Gorczyca, T. W., et al. 2006, ApJS, 167, 343
Bryans, P., Landi, E., & Savin, D. W. 2009, ApJ, 691, 1540
Chen, G. X., Pradhan, A. K., & Eissner, W. 2003, JPhB, 36, 453
Cogordan, J. A., Lunell, S., Jupén, C., & Litzén, U. 1985, PhyS, 31, 545
Culhane, J. L., Harra, L. K., James, A. M., et al. 2007, SoPh, 243, 19
Curdt, W., Landi, E., & Feldman, U. 2004, A&A, 427, 1045
Del Zanna, G. 2008, A&A, 481, L69
Del Zanna, G. 2011, A&A, 536, A59
Del Zanna, G., Dere, K. P., Young, P. R., Landi, E., & Mason, H. E. 2015, A&A, 582, A56
Del Zanna, G., & Ishikawa, Y. 2009, A&A, 508, 1517
Del Zanna, G., & Mason, H. E. 2014, A&A, 565, A14
Dere, K. P., Landi, E., Mason, H. E., Monsignori Fossi, B. C., & Young, P. R. 1997, A&AS, 125, 149
Dong, C., Xie, L., Fritzsche, S., & Kato, T. 2003a, NIMPB, 205, 87
Dong, C. Z., Xie, L. Y., Zhou, X. X., Ma, X. W., & Fritzsche, S. 2003b, HyInt, 146, 161
Dufton, P. 1977, CoPhC, 13, 25
Dyall, K., Grant, I., Johnson, C., Parpia, F., & Plummer, E. 1989, CoPhC, 55, 425
Eissner, W., Jones, M., & Nussbaumer, H. 1974, CoPhC, 8, 270
Feldman, U., Curdt, W., Landi, E., & Wilhelm, K. 2000, ApJ, 544, 508
Froese Fischer, C., & Tachiev, G. 2004, ADNDT, 87, 1
Fuhr, J. R., Martin, G. A., & Wiese, W. L. 1988, JPCRD, 17, 1
Grant, I. P. 2007, Relativistic Quantum Theory of Atoms and Molecules (New York: Springer)
Gu, M. F. 2003, ApJ, 582, 1241
Gu, M. F. 2005a, ADNDT, 89, 267
Gu, M. F. 2005b, ApJS, 156, 105
Gu, M. F. 2007, ApJS, 169, 154
Gu, M. F., Holczer, T., Behar, E., & Kahn, S. M. 2006, ApJ, 641, 1227
Hibbert, A., Ledourneuf, M., & Mohan, M. 1993, ADNDT, 53, 23
Holczer, T., Behar, E., & Kaspi, S. 2005, ApJ, 632, 788
Ishikawa, Y., Encarnación, J. M. L., & Träbert, E. 2009, PhyS, 79, 025301
Ivanova, E. P., & Gulov, A. V. 1991, ADNDT, 49, 1
Jönsson, P., Bengtsson, P., Ekman, J., et al. 2014, ADNDT, 100, 1
Jönsson, P., Gaigalas, G., Bieroń, J., Fischer, C. F., & Grant, I. P. 2013, CoPhC, 184, 2197
Jönsson, P., He, X., Fischer, C. F., & Grant, I. 2007, CoPhC, 177, 597
Kaastra, J. S., Steenbrugge, K. C., Raassen, A. J. J., et al. 2002, A&A, 386, 427
Ko, Y. K., Raymond, J. C., Li, J., et al. 2002, ApJ, 578, 979
Kramida, A., Ralchenko, Yu., Reader, J. & NIST ASD Team 2015, NIST Atomic Spectra Database (ver. 5.3) (Gaithersburg, MD: National Institute of Standards and Technology) available: http://physics.nist.gov/asd [2016, May 10]
Landi, E., & Phillips, K. J. H. 2005, ApJS, 160, 286
Liang, G. Y., & Badnell, N. R. 2010, A&A, 518, A64
Mazzotta, P., Mazzitelli, G., Colafrancesco, S., & Vittorio, N. 1998, A&AS, 133, 403
Mewe, R., Raassen, A., Drake, J., & Kaastra, J. 2001, A&A, 368, 888
Nahar, S. N., Eissner, W., Chen, G.-X., & Pradhan, A. K. 2003, A&A, 408, 789
Ness, J.-U., Brickhouse, N. S., Drake, J. J., & Huenemoerder, D. P. 2003, ApJ, 598, 1277
Paerels, F. B. S., & Kahn, S. M. 2003, ARA&A, 41, 291
Phillips, K. J. H., Fawcett, B. C., Kent, B. J., et al. 1982, ApJ, 256, 774
Quinet, P., Gorlia, T., & Biemont, E. 1991, PhyS, 44, 164
Raassen, A. J. J., Mewe, R., Audard, M., et al. 2002, A&A, 389, 228
Raassen, A. J. J., & Pollock, A. M. T. 2013, A&A, 550, A55
Savukov, I. M. 2003, JPhB, 36, 4789
Shestov, S., Reva, A., & Kuzin, S. 2014, ApJ, 780, 15
Shestov, S. V., Bozhenkov, S. A., Zhitnik, I. A., et al. 2008, AstL, 34, 33
Shirai, T., Sugar, J., Musgrove, A., & Wiese, W. L. 2000, Spectral Data for Highly Ionized Atoms (Melville, NY: AIP)
Si, R., Guo, X., Yan, J., et al. 2015a, JQSRT, 163, 7
Si, R., Guo, X. L., Yan, J., et al. 2015b, JPhB, 48, 175004
Sucher, J. 1980, PhRvA, 22, 348
Wang, K., Guo, X. L., Liu, H. T., et al. 2015, ApJS, 218, 16
Wang, K., Li, D. F., Liu, H. T., et al. 2014, ApJS, 215, 26
Wang, K., Si, R., Dang, W., et al. 2016, ApJS, 223, 3
Warren, H. P., Feldman, U., & Brown, C. M. 2008, ApJ, 685, 1277